Hindawi
International Journal of Aerospace Engineering
Volume 2023, Article ID 5315977, 15 pages
https://doi.org/10.1155/2023/5315977

Research Article

Thermomechanical Behaviors of a Novel Double-Layer Corrugated Core Structure for Thermal Protection System

Bin Li,[1] Zixuan Hang,[2] and Ting Dai[1]

[1]*Research Institute of Aerospace Technology, Central South University, Changsha 410083, China*
[2]*Structural Technology Research Office, Nanjing Changfeng Aerospace Electronic Technology Co., Ltd, Nanjing 211800, China*

Correspondence should be addressed to Ting Dai; daiting90@csu.edu.cn

Received 12 May 2023; Revised 9 June 2023; Accepted 28 June 2023; Published 17 July 2023

Academic Editor: Vijayanandh Raja

Copyright © 2023 Bin Li et al. This is an open access article distributed under the Creative Commons Attribution License, which permits unrestricted use, distribution, and reproduction in any medium, provided the original work is properly cited.

Corrugated core sandwich structures have great potential in the application to thermal protection system of aerospace vehicles. However, the traditional layout of web plates could inevitably lead to thermal short effects and high risk of buckling failure of the integrated thermal protection system (ITPS). In this paper, a novel double-layer ITPS is proposed by splitting and reorganizing a classical corrugated sandwich structure without additional introducing of weight. Distribution types of parallel, symmetric, and orthogonal of the double layers are designed and studied in detail. Basic theory of the thermomechanical problem as well as finite element simulation is carried out to study the responses of the ITPS. Numerical results show that the orthogonal type has more excellent yield resistance at high temperature and large temperature gradient than the others, while the parallel type has a relatively stronger buckling resistance. In addition, the structural stiffness variation caused by temperature dependencies of material parameters is greater than that caused by thermal stress, which shows the significance of consideration of temperature-dependent material properties in structure vibration analysis.

1. Introduction

During the flight of a hypersonic vehicle, especially a reusable launch vehicle, it will be exposed to severe environmental conditions and mechanical loads such as aerodynamic, aerothermal, vibration, and sometimes impact loads [1–3]. Due to the high aerodynamic heating and pressure, a thermal protection system (TPS) becomes one of the most important subsystems for hypersonic vehicles [4–6]. The basic function of a TPS is to avoid thermal failure of the main structure and keep the inside temperature within an acceptable level. An apparent way to improve the thermal insulation ability of a TPS is to enlarge its thickness. However, optimization of mechanical property and structure weight also has to be considered during design of a TPS, as it has significant influences on the overall performance of the flight vehicle. Hence, integrated thermal protection systems (ITPSs) have been invented and attracted widely attentions [7–9]. One classical type of ITPSs is the corrugated core sandwich panel, which consists of two thin surface plates and a corrugated core filled with thermal insulation material [10–12]. Compared with a TPS made of thermal insulation material simply layered between two surface plates, the corrugated core of ITPS keeps the surface plates apart and stabilizes them by resisting vertical deformation, transverse shear strain, and longitudinal curvature [13–15].

Investigations on thermomechanical properties and optimization designs of the corrugated core sandwich ITPSs are easy to find in literature. The Langley Research Center of NASA [16] proposed an improved corrugated sandwich ITPS composed of truss plate and thermal insulation core, of which the thermal short-circuit effect and structure weight were greatly reduced. Based on the corrugated sandwich ITPS, Steeves et al. [17] proposed a multilayer ITPS, but its preparation was complex and the connection process was difficult. Hu et al. [18] designed corrugated lattice truss sandwich panels and observed potential failure modes of structure fracture and bulking in compression. Zhao et al. [19] proposed a corrugated channel sandwich core available for load-bearing and active cooling systems, whose compression performance was better under the same density. Ravishankar et al. [20] carried out thermal and mechanical

analyses with uncertainties for ITPS with double layers. Frostig and Thomsen [21] carried out nonlinear analysis of a delaminated curved sandwich panel with a compliant core, where the delamination is located at one of the face-core interfaces. Ge et al. [22] designed a sandwich structure with bidirectional corrugated core and manufactured by 3D printing. Shi et al. [23] devised and fabricated an all-composite sandwich structure with corrugated core. Zhu et al. [24] designed and developed the analytical models for elastic properties as well as collapse surfaces of an orthogonal corrugated sandwich structure. Xu et al. [25] designed a multilayer ITPS consisting of a carbon fiber-reinforced silicon carbide matrix composite (C/SiC) panel, a glass wool layer, and a titanium (Ti) lattice sandwich filled with glass wool. Shi et al. [26] designed an all-composite sandwich panel with corrugated core which was fabricated using the hot press molding method. Yang et al. [27] reviewed the high performance of an energy absorption capacity with bioinspired sinusoidal corrugated core under quasistatic loads. Sareh [28] studied the design of a developable double corrugation surface that could be employed for transformable structures. Frank et al. [29] presented the influences on mechanical properties of a zigzag-like fold core sandwich structure in a compression test. Ma et al. [30] proposed a combined ITPS consisting of a C/SiC composite corrugated sandwich panel filled with thermal insulation material and an additional thermal insulation layer. Xu et al. [31] minimized the equivalent thermal conductivity and elastic strain energy of the corrugated sandwich panel and established a topology optimization method to deduce a novel core structure.

Though many of the ITPSs in literature perform better than multilayered TPSs in thermomechanical properties, they also have obvious shortcomings. For example, adding weight lightening holes in the web plates is a typical optimizing way for ITPS because of its contributions on weight reduction as well as thermal short-circuit alleviation, but holes will weaken the stiffness and load-bearing capacity of the whole structure. In fact, under the conditions of aerodynamic heating and complex mechanical loads, thermomechanical properties are such important as they usually decide the integrity and security of ITPSs [32–34]. However, from the literature, most of the thermomechanical behavior researches of ITPSs focus on static problems; investigations on dynamic responses are relatively few [35–37]. About 40% of many major accidents of flight vehicle are related to vibration. During flight, the components on the flight vehicle are suffering various vibration loads such as engine vibration and unsteady aerodynamic force. In addition, large temperature gradient and local constraints will cause high thermal stresses in the ITPSs, which may affect the stiffness as well as vibration characteristics of the structure. Hence, a novel type of optimized ITPS will be carried out in this paper, and its dynamic thermomechanical behaviors will be studied in detail.

2. Geometric Structure of the Novel ITPS

The current ITPS is designed based on a classical corrugated core sandwich panel. To avoid introducing additional weight, the following splitting and combining operations are utilized. Splitting part of the top face sheet (TFS) and the bottom face sheet (BFS) and then combining them into one as a middle face sheet (MFS), a double-layer sandwich panel is achieved. Meanwhile, an original web plate is divided into four small web plates, and each layer of the sandwich structure will have four web plates to maintain that the original weight and volume of the whole structure remain unchanged. Therefore, a novel type of double-layer corrugated sandwich panel is structured as shown in Figure 1.

Considering spatial layout of the two layers of the sandwich core, three different types are designed; those are parallel, symmetric, and orthogonal ones. The coordinate system (X, Y, and Z), geometric size parameters, and unit cells of the three types are shown in Figure 2.

3. Thermoelastic Behavior of the Double-Layer Corrugated ITPS

3.1. Governing Equations of the Heat Transfer and Thermoelastic Problems. As the TPS on a hypersonic flight vehicle mainly prevents the high heat flux transferring into the cabin through its thickness, the current analysis will mainly focus on the thickness direction of the ITPS. As shown in Figure 3, an incident heat flux is subjected to the outer surface of the structure, and the inner boundary of the structure exchanges heat freely with the inner environment.

The governing equation of transient heat conduction for a solid body can be written as [38]

$$\rho(T)c(T)\frac{\partial T}{\partial t} = \frac{\partial}{\partial x}\left[k(T)\frac{\partial T}{\partial x}\right] + \frac{\partial}{\partial y}\left[k(T)\frac{\partial T}{\partial y}\right] + \frac{\partial}{\partial z}\left[k(T)\frac{\partial T}{\partial z}\right], \tag{1}$$

where x, y, and z are the coordinates, t is the time, k is the thermal conductivity, ρ is the mass density, c is the specific heat, and T is the temperature.

When $t = 0$, a room temperature is used as initial condition; that is,

$$T(x, y, z, 0) = T_0. \tag{2}$$

Considering the heat exchange between the inner surface and the air inside the cabin, the inner boundary condition should be [38]

$$-k(T)\frac{\partial T}{\partial z}\bigg|_{\text{inner surface}} = h(T_w - T_{\text{in}}), \tag{3}$$

where h is the heat exchange coefficient, T_w is temperature of the inner boundary, and T_{in} is the inside temperature of the cabin.

Considering thermal radiation, the outer boundary condition can be written as [39]

$$-k(T)\frac{\partial T}{\partial z}\bigg|_{\text{outer surface}} - \varepsilon\sigma\left(T_s^4 - T_\infty^4\right) = -q(t), \tag{4}$$

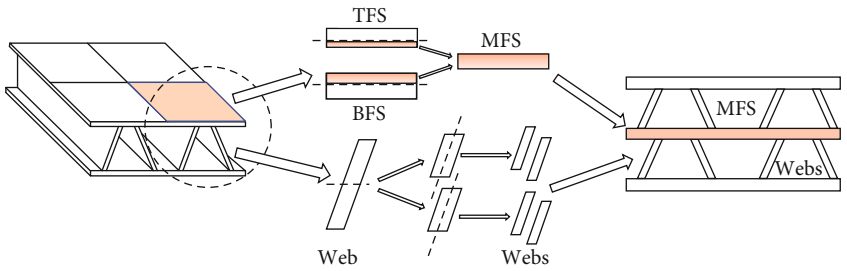

Figure 1: The process of structuring a novel double-layer corrugated sandwich panel by splitting and recombining.

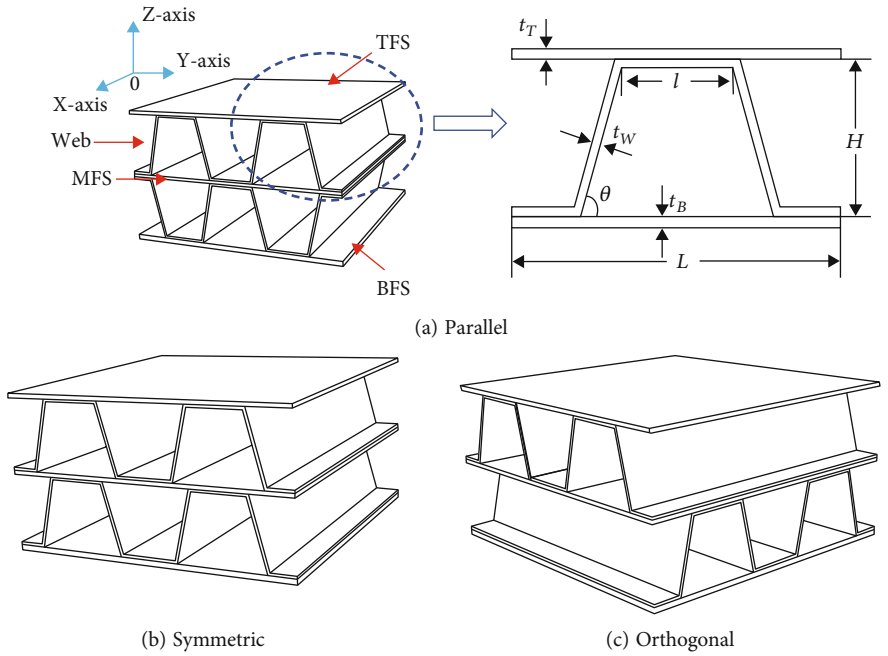

(a) Parallel

(b) Symmetric

(c) Orthogonal

Figure 2: Three types of the double-layer corrugated ITPSs.

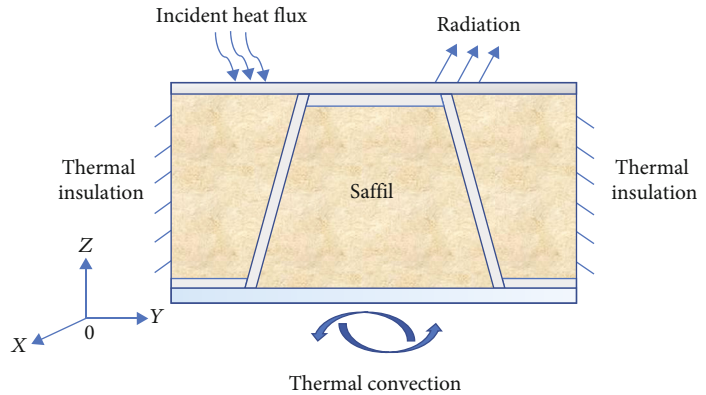

Figure 3: Heat transfer analysis model of the structure.

where ε is the emissivity of the top surface, σ is the Stefan-Boltzmann constant, T_s is the temperature of outer boundary, T_∞ is the outside environment temperature, and $q(t)$ is the heat flux.

According to the linear thermoelastic theory and the generalized Hooke's law, constitutive relation of the structure can be [39–41]

$$\begin{cases} \varepsilon_x = \dfrac{\left[\sigma_x - \mu\left(\sigma_y + \sigma_z\right)\right]}{E} + \alpha\Delta T, \\ \varepsilon_y = \dfrac{\left[\sigma_y - \mu\left(\sigma_z + \sigma_x\right)\right]}{E} + \alpha\Delta T, \\ \varepsilon_z = \dfrac{\left[\sigma_z - \mu\left(\sigma_x + \sigma_y\right)\right]}{E} + \alpha\Delta T, \end{cases} \tag{5}$$

$$\begin{aligned} \gamma_{xy} &= \frac{\tau_{xy}}{G}, \\ \gamma_{yz} &= \frac{\tau_{yz}}{G}, \\ \gamma_{zx} &= \frac{\tau_{zx}}{G}, \end{aligned} \tag{6}$$

where ε_x, ε_y, and ε_z are the normal strains; γ_{xy}, γ_{yz}, and γ_{zx} are the shear strains; and u, v, and w stand for displacements, respectively. α is the thermal expansion, ΔT is the temperature difference, and $\alpha\Delta T$ represents the thermal strain.

Ignoring body force, the equilibrium differential equation should be [39]

$$\begin{cases} \dfrac{\partial\sigma_x}{\partial x} + \dfrac{\partial\tau_{yx}}{\partial y} + \dfrac{\partial\tau_{zx}}{\partial z} = \rho(T)\dfrac{\partial^2 u}{\partial t^2}, \\ \dfrac{\partial\sigma_y}{\partial y} + \dfrac{\partial\tau_{zy}}{\partial z} + \dfrac{\partial\tau_{xy}}{\partial x} = \rho(T)\dfrac{\partial^2 v}{\partial t^2}, \\ \dfrac{\partial\sigma_z}{\partial z} + \dfrac{\partial\tau_{xz}}{\partial x} + \dfrac{\partial\tau_{yz}}{\partial y} = \rho(T)\dfrac{\partial^2 w}{\partial t^2}, \end{cases} \tag{7}$$

where σ_x, σ_y, and σ_z are the corresponding normal stress; τ_{xy}, τ_{yz}, and τ_{xz} are the shear stresses, respectively; E is Young's modulus; G is the shear modulus; and μ is Poisson's ratio.

Considering elastic deformation, the linear geometric equation as follows can be used [39]:

$$\begin{aligned} \varepsilon_x &= \frac{\partial u}{\partial x}, \\ \varepsilon_y &= \frac{\partial v}{\partial y}, \\ \varepsilon_z &= \frac{\partial w}{\partial z}, \end{aligned} \tag{8}$$

$$\begin{aligned} \gamma_{xy} &= \frac{1}{2}\left(\frac{\partial u}{\partial y} + \frac{\partial v}{\partial x}\right), \\ \gamma_{yz} &= \frac{1}{2}\left(\frac{\partial v}{\partial z} + \frac{\partial w}{\partial y}\right), \\ \gamma_{zx} &= \frac{1}{2}\left(\frac{\partial w}{\partial x} + \frac{\partial u}{\partial z}\right). \end{aligned} \tag{9}$$

Combining Equation (5)~Equation (9), the governing equations expressed by displacements u, v, and w can be achieved. To solve the thermomechanical problem, the following boundary conditions will be applied.

A time-dependent pressure caused by aerodynamic phenomenon will be considered on the outer surface of the structure as

$$\sigma_z\big|_{\text{outer surface}} = p(t). \tag{10}$$

To simulate the connections between the calculated structure and the surround parts, some necessary constrains of displacements will be applied, and the detail information will be stated in the following section where the numerical model is described.

3.2. Numerical Results of the Temperature and Stress Distributions. The commercial finite element software Abaqus is used for numerical calculation. As the heat conduction and thermomechanical behavior are both investigated in detail in this paper, a sequentially coupled analysis method is used. That is, a transient heat conduction step is applied and solved to achieve the time-dependent temperature field, and then, the temperature results will be used as a predefined field in the mechanic step.

Before the numerical examples, a validation example to show the correctness of the simulation process of the current work is carried out. A simplified corrugated core sandwich plane is modeled here, of which the geometrical shape, sizes, material parameters, and thermal loads are all the same as those in Ref. [42]. Figure 4 shows comparison of the results in the reference and calculated by the numerical process of this paper. Obviously, the results are close enough (with a maximum deviation of about 2.75%) to indicate the correctness and reliability of the numerical process of this paper.

For the current analysis, the titanium alloy (Ti-6Al-4V) is used for the top, bottom, and middle face sheets as well as the web plates. The temperature-dependent material properties of Ti-6Al-4V are listed in Table 1 [43], and its Poisson's ratio is 0.31. The sandwich core is filled with Saffil fibrous thermal insulation material whose temperature-dependent material properties are given in Table 2 [43].

The heat flux subjecting to the outer surface of the structure is assumed to vary along time as shown in Figure 5, and the aerodynamic pressure is given in Figure 6 [44]. Radiation emissivity of the outer surfaces is set to be 0.8, and heat exchange coefficient of the inner surface is set to be 15. Note that perfect interfaces between various materials are considered in the current model; hence, thermal contact resistance is ignored.

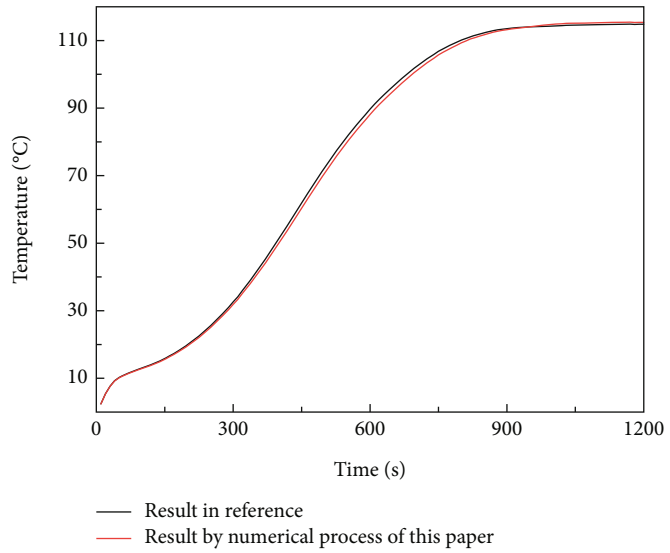

Figure 4: Comparison of the results in Ref. [42] and calculated by the numerical process of this paper for a simplified model.

Table 1: Temperature-dependent material property parameters of Ti-6Al-4V [43].

T (°C)	ρ (kg·m^{-3})	k (W)/(m·K)$^{-1}$	c (J)/(kg·K)$^{-1}$	E (GPa)	α (10^{-6}·K^{-1})
0	4429	7.0	562	110.9	8.65
50	4429	7.4	549	108.0	8.82
150	4429	8.1	557	100.5	9.16
250	4429	9.4	591	93.8	9.44
350	4429	10.9	629	86.9	9.73
450	4429	12.2	673	79.6	10.0
550	4429	13.4	725	53.3	10.2
650	4429	14.4	780	44.0	10.3
750	4429	15.2	860	32.6	10.3
850	4429	15.8	928	21.1	10.3

Table 2: Temperature-dependent material property parameters of Saffil [43].

T (°C)	k (W)/(m·K)$^{-1}$	c (J)/(kg·K)$^{-1}$
100	0.02669	724.32
200	0.02916	950.4
300	0.04359	1021.58
400	0.06251	192.75
500	0.08673	1138.81
600	0.11739	1172.3
700	0.15402	1197.42
800	0.19813	1222.55
900	0.24972	1239.29
1000	0.30879	1251.85
1100	0.37683	1260.23
1200	0.45309	1268.6
1300	0.53833	1472.75

In the following numerical examples, geometric sizes of the structure are listed in Table 3, where the meaning of each parameter is shown in Figure 2(a).

Note that the thermal insulation material filled in the sandwich core is a kind of soft and flexible cotton wool material with low density, of which the stiffness is extremely low compared with the other parts of the ITPS. Therefore, in the following analysis, thermal insulation material will only be modeled in the calculation of temperature filed, while be ignored when investigating the load-bearing performance of the structure.

To save computing resources, only a small typical part of the whole structure is modeled. The mechanical load and boundary conditions are shown in Figure 7, where the detail boundary conditions (BCs) are set as follows:

BC I and II: symmetric boundaries, to simulate the connection between the modeled part and the surrounded parts with identical structure;

BC III: the displacements are constrained, to simulate the connection between the modeled part and the cabin of the flight vehicle.

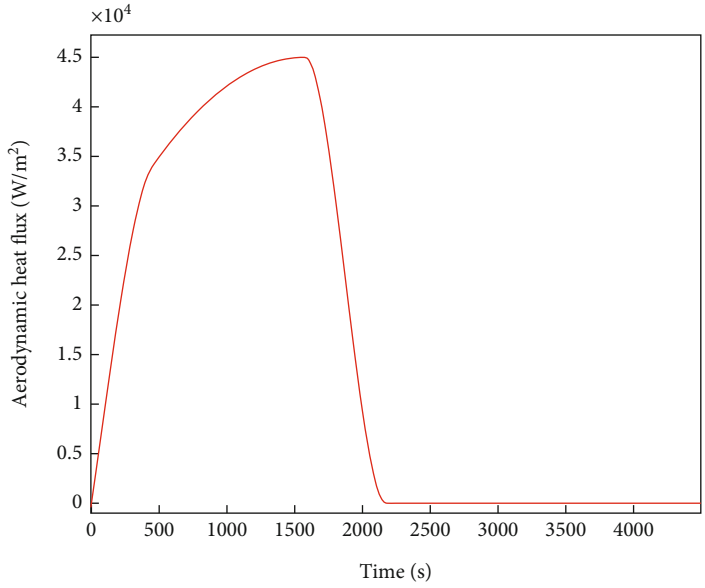

Figure 5: Aerodynamic heat flux of a typical hypersonic cruise vehicle [44].

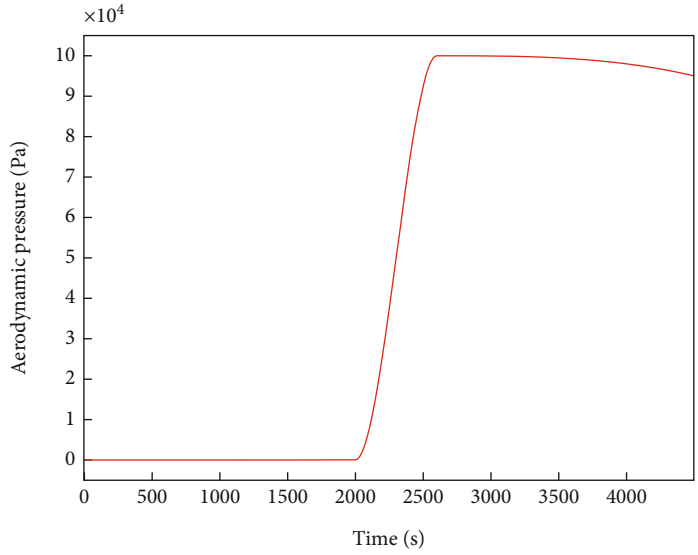

Figure 6: Aerodynamic pressure of a typical hypersonic cruise vehicle [44].

Table 3: Geometric parameters of the structure.

Parameters	t_T (mm)	t_B (mm)	t_W (mm)	L (mm)	H (mm)	θ (°)
Sizes	2	3	1.5	80	40	76

As the model is relatively simple, the type of structured grid is used. To verify the grid independence of the numerical results, a model including 1/4 part of the structure (the left in Figure 7) is built and the temperature field is calculated under different mesh size. Figure 8 shows the temperature results at the bottom of the 1/4 model separately using the grid sizes 1.0 mm, 0.5 mm, and 0.1 mm. Obviously, the difference is small enough to indicate the grid independence. Hence, in the following numerical examples, grid sizes about 1.0 mm will be used to save computing resources.

Figure 9 shows the maximum stress and displacement fields of the three designed structure types. It can be seen that the maximum stress value of the orthogonal type is 721 MPa, which is 399 MPa and 182 MPa less than the parallel and symmetric types, respectively. The maximum stress of the parallel type exceeds the allowable stress of the

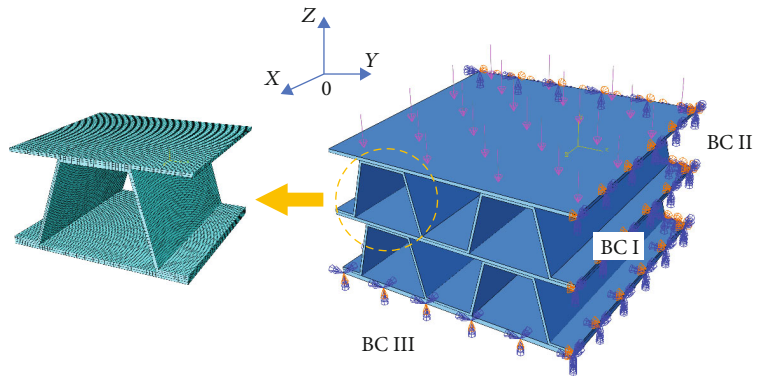

Figure 7: Analysis model of a parallel ITPS with the thermal insulation material hided.

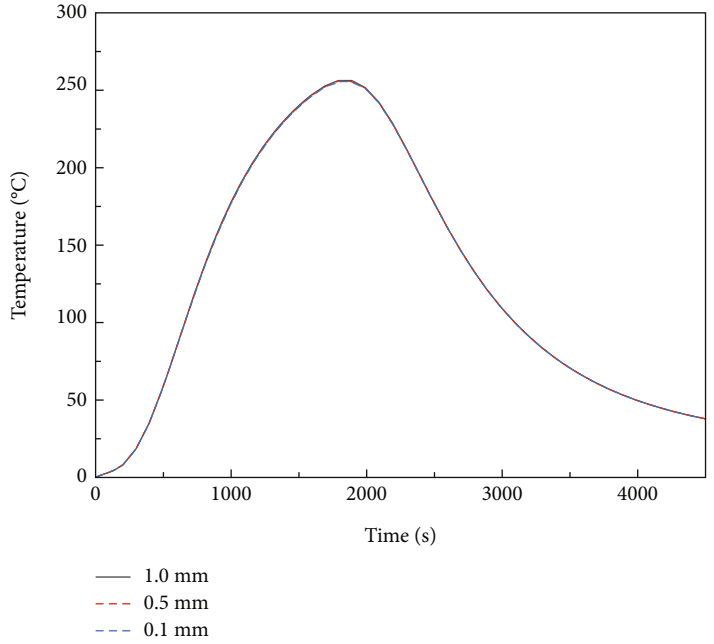

Figure 8: The temperature results at the bottom of the 1/4 model using different gird sizes.

material. For the location where the maximum stress occurs, the one of parallel occurs at the junction of the middle face sheet and the upper web plate, while the ones of the other two types occur near the bottom face sheets. For the maximum displacement, the three schemes have little difference. The position of maximum displacement happens at the corner of the top face sheet.

Figure 10 shows variations of the maximum stresses and displacements along time of the three types of ITPSs. It can be seen that the maximum stresses of the three schemes have little difference after 2500 s. In the range of 1000 s~2500 s, the maximum stress value of the orthogonal type is lower than the parallel and symmetric types, which may tell that the orthogonal type has the best yield resistance under high temperature and large temperature gradient.

Figure 11 shows the first-order buckling modes as well as the buckling eigenvalues of each scheme. At the moment of maximum temperature gradient, the thermal mismatch effect is the most obvious, and at the moment of maximum back temperature, the mechanical performance of the lower wall is the weakest. Therefore, the structure is prone to buckling deformation in these two states. The buckling eigenvalues of the three schemes are greater than 1, indicating that structural buckling will not occur in reentry environment. This is because the sandwich layer is separated by the middle face sheet, and the height of each sandwich layer is reduced to half when splitting and recombining. When the web plate thickness is a fixed value, the ratio of it to the height of each sandwich layer increases, resulting in the increase of buckling failure stress. In addition, the existence of the middle face sheet increases the transverse heat conduction and inhibits the heat transfer of the overall structure from outside to inside.

From the above numerical results, it can be known that the buckling eigenvalue of the parallel type is the largest, which means the parallel type has the largest critical load

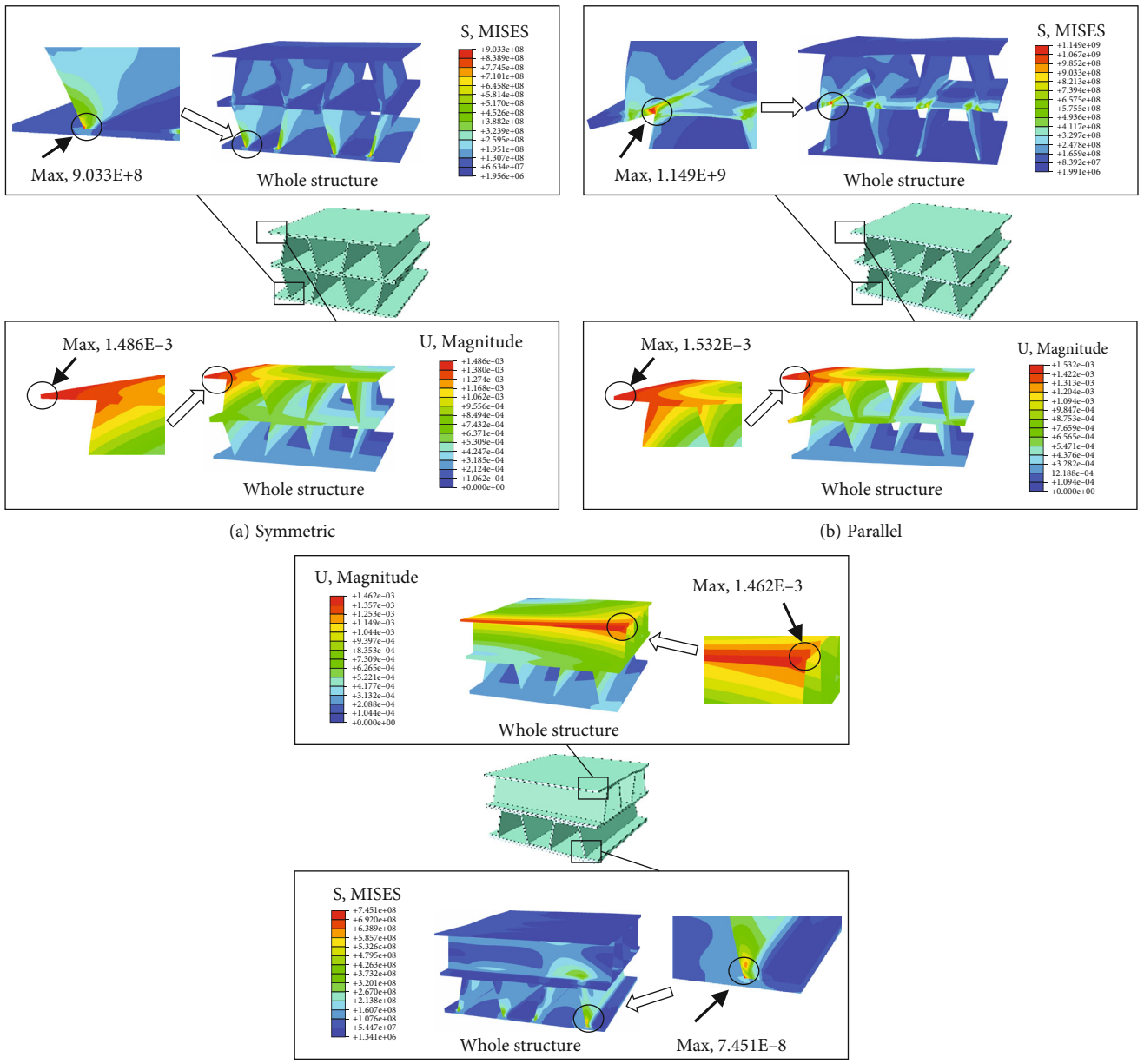

Figure 9: Thermal stress and displacement fields of various double-layer ITPSs.

and relatively stronger buckling resistance property. This is because deformation constraint of the web plate of the parallel type is weaker than the other two structures, due to the possible displacement of the end of the web plate during bending of the middle face sheet.

4. Free Vibration of the Double-Layer Corrugated ITPS under Thermal Environment

4.1. Governing Equations of the Free Vibration Problem. Free vibration analysis is of great importance for a dynamical problem, which can reveal the inherent properties of the designed structure, especially the effect of thermal environment on its vibration modes. Hence, after obtaining the temperature and thermal stress distributions, this section further carries out the thermal modal analyses as well as the free vibration characteristics of the structures.

Equation (5)~Equation (9) can also be used to derive the governing equation for free vibration when ignoring the damping force. Applying the finite element method, the governing equation can be discretized and expressed by the nodal displacements as [45]

$$\mathbf{M}_T\ddot{\mathbf{u}}_t + \mathbf{K}_T\mathbf{u}_t = \mathbf{0}, \tag{11}$$

where $\mathbf{u}_t$ is the nodal displacement matrix. $\mathbf{M}_T$ and $\mathbf{K}_T$ are separately the mass and stiffness matrix. Note that, in the current problem, both the mass matrix and the stiffness

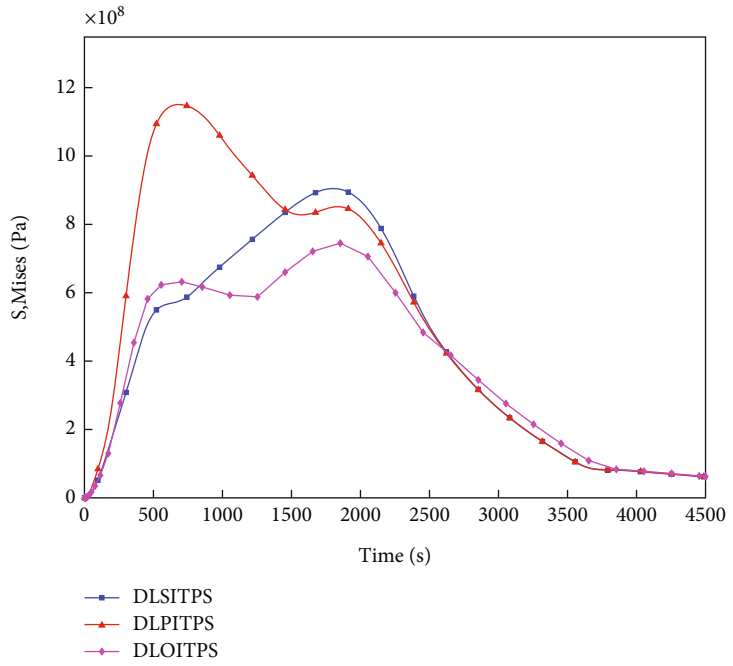

(a) Maximum stress

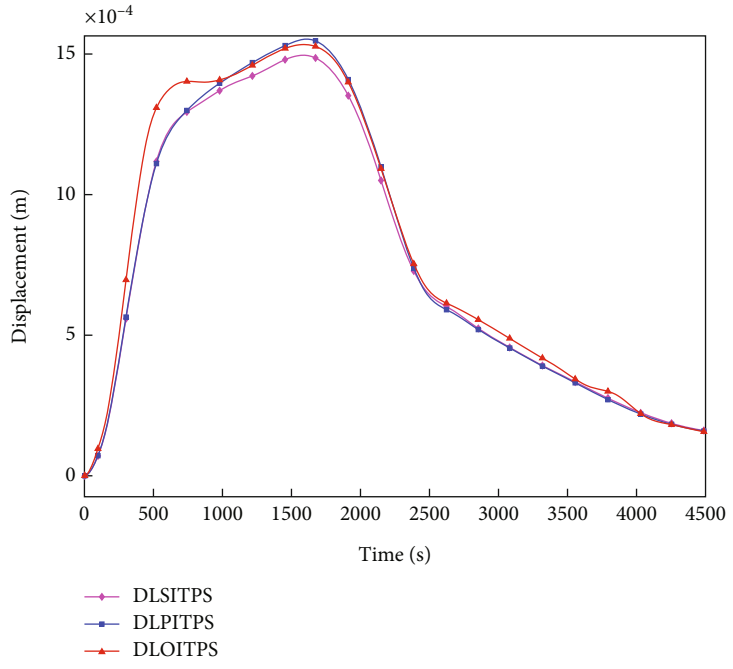

(b) Maximum displacement

FIGURE 10: Maximum stresses and displacements of various ITPSs along time.

matrix are temperature dependent. Substituting the harmonic solution $\mathbf{u}_t = \hat{\mathbf{u}}e^{i\omega t}$ into the governing equation, the eigen equation can be obtained as [45]

$$\left|\left(\mathbf{K}_T - \omega^2 \mathbf{M}_T\right)\right| = \mathbf{0}. \tag{12}$$

Then, natural circular frequency ω as well as the free vibration mode can be achieved by solving the above equations, and the effect of temperature field on the vibration properties can be discussed.

4.2. Numerical Results of the Free Vibration Response under Thermal Environment. Compared with other structural forms, the orthogonal arrangement structure has great advantages in load-bearing performance. Therefore, this section only analyzes the vibration performance of the orthogonal type in thermal environment. Figure 12 shows the first

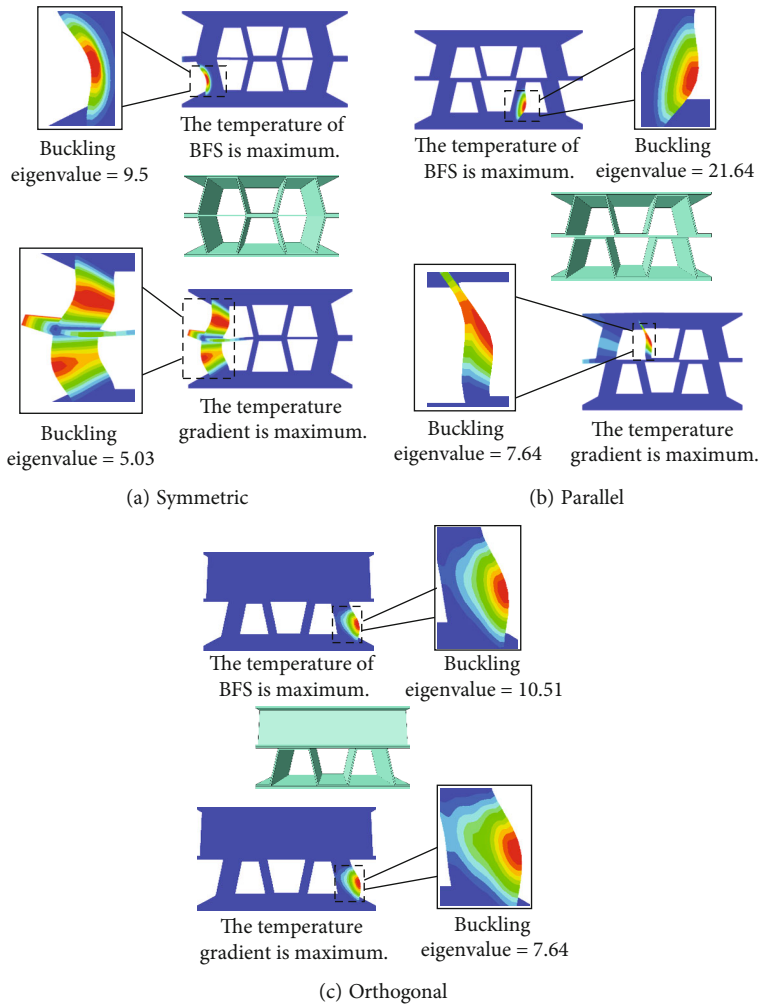

Figure 11: Buckling modes and eigenvalues of structures.

six thermal modes of orthogonal panel under 200°C uniform temperature field. It can be found that the modal vibration modes of the first five orders have little difference in general. The darker red parts are the areas where the larger waveform amplitudes appear. It can be seen that the maximum waveform amplitude is located at the center. With the increase of order, the initial waveforms are gradually divided into multiple strip modal waveforms of in-phase vibration with the same shape; that is, the waveforms are splitting in-phase and the direction is symmetrically left and right due to the symmetries of both structure and temperature field.

Figure 13 shows the first six natural frequency changes of the panel under uniform temperature fields. It can be found that with the increase of temperature, the natural frequencies show a monotonic decreasing trend, which is the direct influence of material softening effect. The structural stiffness caused by thermal stress is less than the one that decreases with the reduction of material properties, which leads to the decrease of the overall stiffness. In detail, when it is lower than 400°C, the decrease trend is gradual, while after exceeding 400°C, the trend is relatively more dramatic. This is because the elastic modulus of the panel material decreases with the increase of temperature, and this kind of influence becomes more obvious under higher temperature.

In the following, referring to the real aerodynamic heating time and considering simply supported boundaries, the structural modes under nonuniform temperature fields and the influences of temperature gradients on the natural modal characteristics are studied. The loaded temperatures here are the achieved temperature fields of the structure at 260 s, 320 s, 450 s, 1600 s (when the maximum temperature gradient occurs), 2000 s (when the maximum temperature of the inside boundary occurs), 2650 s, 3000 s, 3600 s, and 4000 s in the preceding section. The magnitudes of temperature gradient at these nine time points are ordered as follows:

$$\Delta T|_{t=4000\mathrm{s}} < \Delta T|_{t=3600\mathrm{s}} < \Delta T|_{t=2650\mathrm{s}} < \Delta T|_{t=3000\mathrm{s}} < \Delta T|_{t=320\mathrm{s}} < \Delta T|_{t=260\mathrm{s}} < \Delta T|_{t=2000\mathrm{s}} < \Delta T|_{t=450\mathrm{s}} < \Delta T|_{t=1600\mathrm{s}}. \quad (13)$$

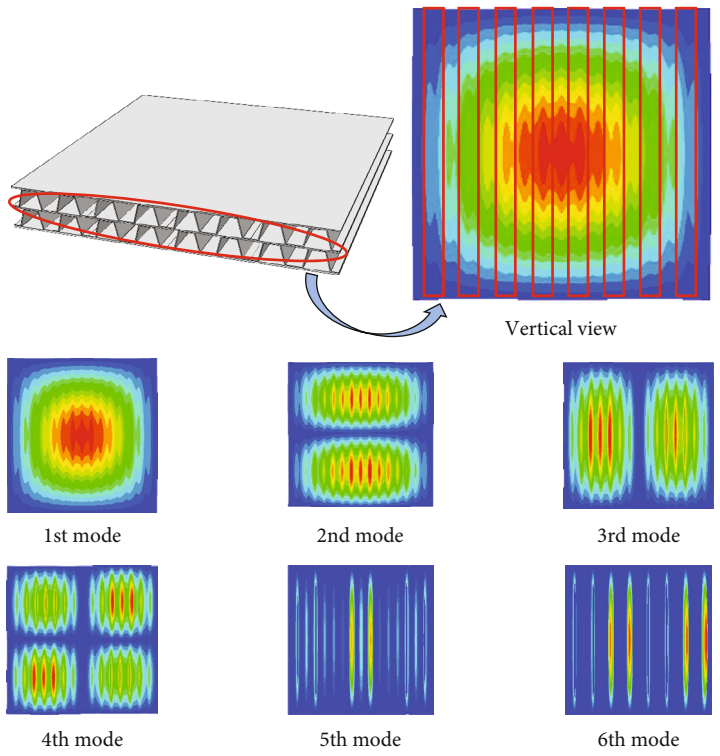

Figure 12: Natural mode shapes of the first six thermal modes of the orthogonal type under 200°C uniform temperature field.

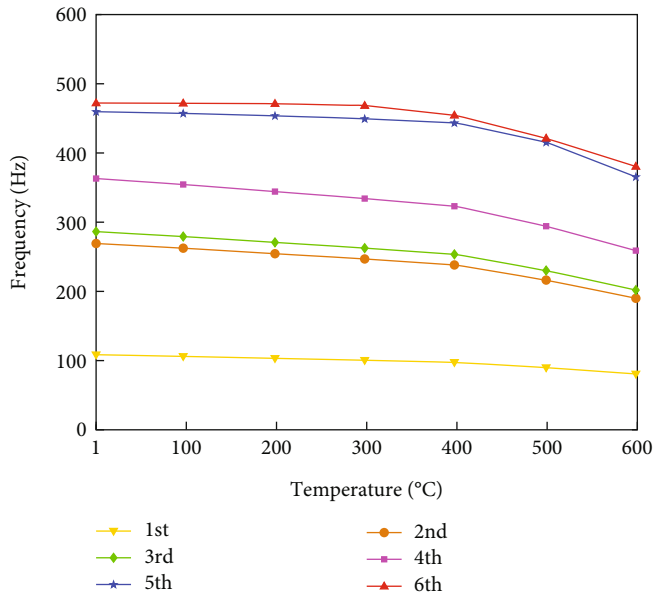

Figure 13: The first six natural frequencies under different uniform temperature fields.

The increment of temperature gradient is represented by number

$$\Delta T_1 < \Delta T_2 < \Delta T_3 < \Delta T_4 < \Delta T_5 < \Delta T_6 < \Delta T_7 < \Delta T_8 < \Delta T_9. \quad (14)$$

Figure 14 shows the first six thermal modes at the time of maximum temperature gradient. The first four modes are almost the same as those in Figure 12, while the fifth order is three strip waveforms symmetrically up and down, and then, each waveform separately splits left and right in phase and gradually changes into six smaller block waveforms in

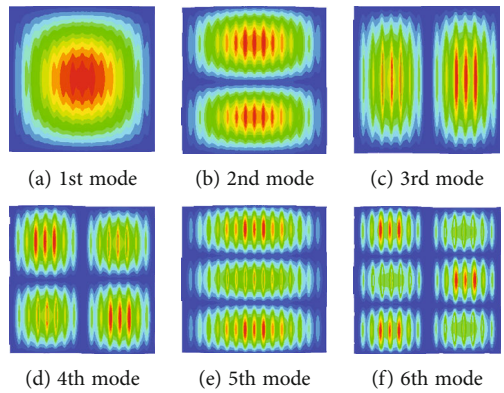

Figure 14: Natural mode shapes of the first six thermal modes of the orthogonal type when the maximum temperature gradient occurs.

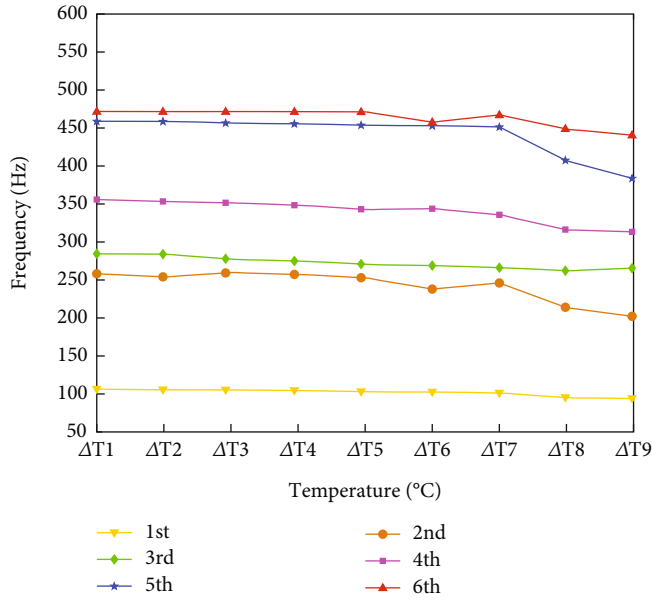

Figure 15: The first six natural frequencies under different temperature gradients.

the sixth mode. At the same time, compared with the high-order mode, the phenomenon of large waveform amplitude is more obvious, indicating that the existence of temperature gradient will significantly affect the high-order mode of the orthogonal type.

Figure 15 shows the natural frequencies under different time points. The temperature gradient corresponding to each flight time of the coordinate axis changes in an increasing trend. It can be seen from the figure that the natural frequency of the orthogonal type no longer decreases monotonically but increases slightly in the middle. This is because the stiffness hardening effect of the structure is gradually enhanced due to the existence of aerodynamic pressure and thermal deformation. The stiffness hardening caused by deformation plays a major role, so that the natural frequency of the structure rises slightly with the increase of temperature gradient. The stiffness of the structure is enhanced.

The above analysis shows that aerodynamic heating for a long time will have a great impact on the natural vibration characteristics of the structure. Among them, the internal stress caused by aerodynamic force and temperature gradient may enhance the stiffness of the structure.

According to Equations (11) and (12), the stiffness is temperature dependent due to the changes of material parameters along the rise of temperature as well as the thermal stress under displacement constrains. In order to study the effect of temperature dependency on the free vibration properties, comparison examples are carried out in Figures 16 and 17. Two cases are assumed here as ignoring temperature dependencies of material parameters (utilizing the constant parameters at 200°C) and ignoring the thermal stress.

It can be seen from Figure 16 that when the above two terms are both considered, the frequency has the lowest level, while when temperature dependencies of material parameters are ignored, the frequency has the highest level. Figure 17 shows the sixth natural frequency under different uniform temperature fields as 0°C, 100°C, 200°C, and 300°C with the above conditions. It is easily found that the

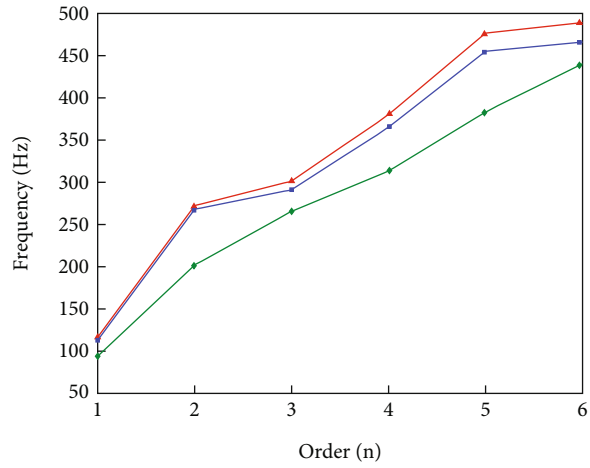

Figure 16: Comparison of the frequencies under different assumptions.

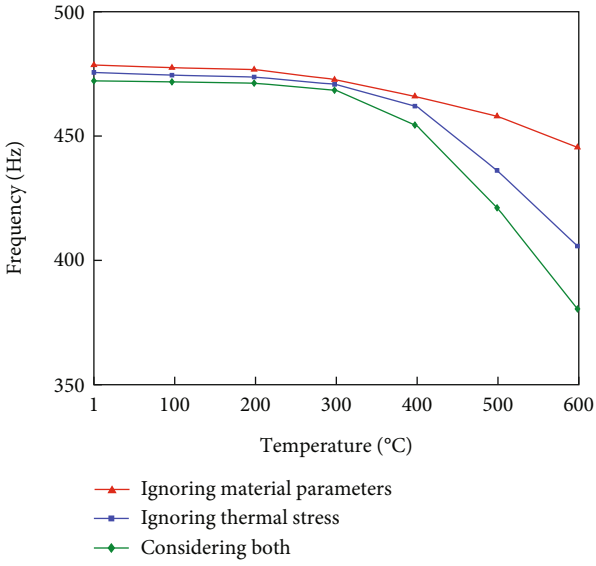

Figure 17: The 6th order natural frequency under uniform temperature fields with different assumptions.

temperature dependencies of material parameters have greater influence on the natural frequency than thermal stress. These results may tell the significance of consideration of temperature dependencies for material properties when investigating the structural vibration characteristics under thermal environment.

5. Conclusion

In this paper, a novel double-layer corrugated core structure for ITPS is proposed by splitting and reorganizing, and its thermomechanical behaviors are studied in detail. The thermal stress, displacement, buckling, and free vibration of the structure are studied. Influence of thermal environment on the dynamic characteristics and dynamic responses of the structure are discussed by numerical examples. Several key conclusions obtained are listed as follows:

(1) The orthogonal type has more excellent yield resistance at high temperature and large temperature gradient than the parallel and symmetric types. The buckling eigenvalue of the parallel type is the largest among the three types, which means the parallel type has a relatively stronger buckling resistance

(2) Under a uniform temperature field, the natural frequencies show a monotonic decreasing trend with the increase of temperature, and when the temperature exceeds 400°C, this trend is more obvious. Under a nonuniform temperature field, the natural frequency of the structure rises slightly with the increase of temperature gradient

(3) Comparing the effect of two stiffness terms, the structural stiffness variation caused by temperature dependencies of material parameters is greater than that caused by thermal stress, which shows the significance of consideration of temperature-dependent material properties in structure vibration analysis

Data Availability

The data used to support the findings of this study are available from the corresponding author upon reasonable request.

Conflicts of Interest

The authors declare that they have no conflicts of interest.

Acknowledgments

This work is funded by the National Natural Science Foundation of China (no. 12102486) and the Hunan Provincial Innovation Foundation for Postgraduate (no. CX20220307).

References

[1] G. Xie, R. Zhang, and O. Manca, "Thermal and thermomechanical performances of pyramidal core sandwich panels under aerodynamic heating," *Journal of Thermal Science and Engineering Applications*, vol. 9, no. 1, article 014503, 2017.

[2] V. T. Le and N. S. Goo, "Thermomechanical performance of bio-inspired corrugated-core sandwich structure for a thermal protection system panel," *Applied Sciences*, vol. 9, no. 24, p. 5541, 2019.

[3] T. Suzuki, T. Aoki, T. Ogasawara, and K. Fujita, "Nonablative lightweight thermal protection system for Mars Aeroflyby sample collection mission," *Acta Astronautica*, vol. 136, pp. 407–420, 2017.

[4] S. Meng, Q. Yang, W. Xie, G. Han, and S. Du, "Structure redesign of the integrated thermal protection system and fuzzy performance evaluation," *AIAA Journal*, vol. 54, no. 11, pp. 3598–3607, 2016.

[5] T. Boonkong, Y. O. Shen, Z. W. Guan, and W. J. Cantwell, "The low velocity impact response of curvilinear-core sandwich structures," *International Journal of Impact Engineering*, vol. 93, pp. 28–38, 2016.

[6] M. Olivero, M. Ferrai, P. Pantaleone et al., "Lumped parameter modelling for the thermal analysis of the launch vehicle Vega C," *Aircraft Engineering and Aerospace Technology*, vol. 90, no. 3, pp. 542–558, 2018.

[7] W. Zhuang, C. Yang, and Z. Wu, "Modal and aeroelastic analysis of trapezoidal corrugated-core sandwich panels in supersonic flow," *International Journal of Mechanical Sciences*, vol. 157-158, pp. 267–281, 2019.

[8] C. Gogu, S. K. Bapanapalli, R. T. Haftka, and B. V. Sankar, "Comparison of materials for an integrated thermal protection system for spacecraft reentry," *Journal of Spacecraft and Rockets*, vol. 46, no. 3, pp. 501–513, 2009.

[9] H. Linshu and X. Dajun, "Optimal trajectory analysis of hypersonic boost-glide waverider with heat load constraint," *Aircraft Engineering and Aerospace Technology: An International Journal*, vol. 87, no. 1, pp. 67–78, 2015.

[10] D. Tumino, T. Ingrassia, V. Nigrelli, G. Pitarresi, and V. U. Miano, "Mechanical behavior of a sandwich with corrugated GRP core: numerical modeling and experimental validation," *Frattura ed Integrità Strutturale*, vol. 8, no. 30, pp. 317–326, 2014.

[11] S. Meng, Q. Yang, W. Xie, C. Xu, and H. Jin, "Comparative study of structural efficiencies of typical thermal protection concepts," *AIAA Journal*, vol. 55, no. 7, pp. 2476–2480, 2017.

[12] I. Dayyani, M. I. Friswell, S. Ziaei-Rad, and E. S. Flores, "Equivalent models of composite corrugated cores with elastomeric coatings for morphing structures," *Composite Structures*, vol. 104, pp. 281–292, 2013.

[13] Y. Yu, W. Hou, P. Hu, H. Yang, and X. Jia, "Failure analysis and bending performance of carbon fiber composite sandwich structures with corrugated cores," *Journal of Sandwich Structures & Materials*, vol. 23, no. 5, pp. 1427–1452, 2021.

[14] T. Fu, Z. Chen, H. Yu, C. Li, and Y. Zhao, "Thermal buckling and sound radiation behavior of truss core sandwich panel resting on elastic foundation," *International Journal of Mechanical Sciences*, vol. 161-162, article 105055, 2019.

[15] R. P. Yu, X. Wang, Q. C. Zhang et al., "Effects of sand filling on the dynamic response of corrugated core sandwich beams under foam projectile impact," *Composites Part B: Engineering*, vol. 197, article 108135, 2020.

[16] M. L. Blosser, K. Daryabeigi, R. K. Bird, and J. R. Knutson, *Transient Thermal Testing and Analysis of a Thermally Insulating Structural Sandwich Panel*, NASA/TM-2015-218701, 2015.

[17] C. A. Steeves, M. He, P. T. Maxwell, and A. G. Evans, "Design of a robust, multifunctional thermal protection system incorporating zero expansion lattices," in *Proceedings of the ASME 2007 International Mechanical Engineering Congress and Exposition. Volume 1: Advances in Aerospace Technology*, pp. 255–260, Seattle, Washington, USA, November 2007.

[18] Y. Hu, W. Li, X. An, and H. Fan, "Fabrication and mechanical behaviors of corrugated lattice truss composite sandwich panels," *Composites Science and Technology*, vol. 125, pp. 114–122, 2016.

[19] Z. Zhao, J. Ren, S. Du et al., "Bending response of 3D-printed titanium alloy sandwich panels with corrugated channel cores," *Materials*, vol. 14, no. 3, p. 556, 2021.

[20] B. Ravishankar, R. Haftka, and B. Sankar, "Uncertainty analysis of integrated thermal protection system with rigid insulation bars," in *52nd AIAA/ASME/ASCE/AHS/ASC Structures, Structural Dynamics and Materials Conference*, Denver, Colorado, USA, April 2011.

[21] Y. Frostig and O. Thomsen, "Geometrically nonlinear thermomechanical response of circular sandwich plates with a compliant core," *Journal of Mechanics of Materials and Structures*, vol. 6, no. 6, pp. 925–948, 2011.

[22] L. Ge, H. Zheng, H. Li, B. Liu, H. Su, and D. Fang, "Compression behavior of a novel sandwich structure with bi-directional corrugated core," *Thin-Walled Structures*, vol. 161, article 107413, 2021.

[23] S. Shi, Y. Chen, C. Dai, and J. Liang, "Modeling the high temperature behavior of all-composite, corrugated-core sandwich panels undergoing ablation," *Thin-Walled Structures*, vol. 164, article 107742, 2021.

[24] Y. Zhu, Q. Qin, and J. Zhang, "On effective mechanical properties of an orthogonal corrugated sandwich structure," *Materials & Design*, vol. 201, article 109491, 2021.

[25] Y. Xu, N. Xu, W. Zhang, and J. Zhu, "A multi-layer integrated thermal protection system with C/SiC composite and Ti alloy lattice sandwich," *Composite Structures*, vol. 230, article 111507, 2019.

[26] S. Shi, Y. Wang, L. Yan, P. Sun, M. Li, and S. Tang, "Coupled ablation and thermal behavior of an all-composite structurally integrated thermal protection system: fabrication and modeling," *Composite Structures*, vol. 251, article 112623, 2020.

[27] F. Yang, S. Cheng, T. Zeng et al., "Mechanical and oxidation properties of C/SiC corrugated lattice core composite sandwich panels," *Composite Structures*, vol. 158, pp. 137–143, 2016.

[28] P. Sareh, "The least symmetric crystallographic derivative of the developable double corrugation surface: computational design using underlying conic and cubic curves," *Materials & Design*, vol. 183, article 108128, 2019.

[29] C. P. Frank, O. J. Pinon-Fischer, and D. N. Mavris, "A flexible multi-disciplinary environment for performance, life-cycle cost, and safety evaluation of suborbital vehicles," *Aerospace Science and Technology*, vol. 77, pp. 555–562, 2018.

[30] Y. Ma, B. Xu, M. Chen et al., "Optimization design of built-up thermal protection system based on validation of corrugated core homogenization," *Applied Thermal Engineering*, vol. 115, pp. 491–500, 2017.

[31] Q. Xu, S. Li, and Y. Meng, "Optimization and re-design of integrated thermal protection systems considering thermomechanical performance," *Applied Sciences*, vol. 11, no. 15, p. 6916, 2021.

[32] Q. Wu, A. Vaziri, M. E. Asl et al., "Lattice materials with pyramidal hierarchy: systematic analysis and three dimensional failure mechanism maps," *Journal of the Mechanics and Physics of Solids*, vol. 125, pp. 112–144, 2019.

[33] G. Gao, J. J. Gou, C. L. Gong, J. X. Hu, and R. C. Gao, "A novel mechanical-thermal-electrical thermal protection system concept and its multi-scale performance evaluation for hypersonic launch vehicles," *Composite Structures*, vol. 268, article 113962, 2021.

[34] Y. Rong, W. Luo, J. Liu, Z. Shen, and W. He, "Effect of core materials on the low-velocity impact behaviour of trapezoidal corrugated sandwich panels," *International Journal of Crashworthiness*, vol. 25, no. 5, pp. 505–516, 2020.

[35] H. Abedzade Atar, M. Zarrebini, H. Hasani, and J. Rezaeepazhand, "Free vibration analysis of integrated and non-integrated corrugated core sandwich panels reinforced with weft-knitted fabrics," *Journal of Sandwich Structures & Materials*, vol. 23, no. 5, pp. 1571–1593, 2021.

[36] L. Gu, Y. Wang, S. Shi, and C. Dai, "An approach for bending and transient dynamic analysis of integrated thermal protection system with temperature-dependent material properties," *Composite Structures*, vol. 159, pp. 128–143, 2017.

[37] O. A. Martinez, B. V. Sankar, R. T. Haftka, S. K. Bapanapalli, and M. L. Blosser, "Micromechanical analysis of composite corrugated-core sandwich panels for integral thermal protection systems," *AIAA Journal*, vol. 45, no. 9, pp. 2323–2336, 2007.

[38] S. Z. Feng, X. Y. Cui, and G. Y. Li, "Transient thermal mechanical analyses using a face-based smoothed finite element method (FS-FEM)," *International Journal of Thermal Sciences*, vol. 74, pp. 95–103, 2013.

[39] M. R. Eslami, R. B. Hetnarski, J. Ignaczak, N. Noda, N. Sumi, and Y. Tanigawa, *Theory of Elasticity and Thermal Stresses*, Springer, Dordrecht, 2013.

[40] T. Dai, B. Li, C. Tao, Z. He, and J. Huang, "Thermo-mechanical analysis of a multilayer hollow cylindrical thermal protection structure with functionally graded ultrahigh-temperature ceramic to be heat resistant layer," *Aerospace Science and Technology*, vol. 124, article 107532, 2022.

[41] T. Dai, Y. Wei, C. Tao, and J. Huang, "Mechanical model of stiffness coefficients prediction of curved fiber reinforced composites considering fiber distribution and aggregation," *Composite Structures*, vol. 321, article 117277, 2023.

[42] Y. Li, L. Zhang, R. He et al., "Integrated thermal protection system based on C/SiC composite corrugated core sandwich plane structure," *Aerospace Science and Technology*, vol. 91, pp. 607–616, 2019.

[43] B. Han, K. K. Qin, Q. C. Zhang, Q. Zhang, T. J. Lu, and B. H. Lu, "Free vibration and buckling of foam-filled composite corrugated sandwich plates under thermal loading," *Composite Structures*, vol. 172, pp. 173–189, 2017.

[44] Q. Yang, B. Gao, Z. Xu, W. Xie, and S. Meng, "Topology optimisations for integrated thermal protection systems considering thermo-mechanical constraints," *Applied Thermal Engineering*, vol. 150, pp. 995–1001, 2019.

[45] C. Tao and T. Dai, "Large amplitude free vibration of porous skew and elliptical nanoplates based on nonlocal elasticity by isogeometric analysis," *Mechanics of Advanced Materials and Structures*, vol. 29, no. 18, pp. 2652–2667, 2022.